RSC Advances

PAPER

View Article Online
View Journal | View Issue

Cite this: *RSC Adv.*, 2023, **13**, 5317

Two-photon absorption behavior of conjugated oligomers suitable for low colour temperature LEDs†

Tianhao Huang, *[a] Chengzi Jiang,[b] Tianning Xu,*[a] Jinhui Ying,[a] Ran Lu [c] and Huipeng Zhou*[d]

Received 5th January 2023
Accepted 7th February 2023

DOI: 10.1039/d3ra00083d

rsc.li/rsc-advances

Light emitting diodes (LEDs) with low colour temperatures (CTs) have been proved to be physiologically-friendly light sources. However, there are few reports on the photophysical properties of luminescent materials with CTs lower than candlelight. Herein, one- and two-photon optical properties of four fluorenone-based conjugated oligomers have been systemically investigated. By using a sum-over-essential states (SOS) approach, we obtained the transition dipole moments and two-photon absorption (TPA) cross sections. The triphenylamine end-capped oligomer exhibits reddish orange luminescence with extremely low colour temperature of 1686 K, which is much lower than that of candlelight. Fluorene–ethylene units serving as π-spacers could weaken the role of electron-donating units and effectively enhance the TPA performance of oligomers. Our results provide an effective way for the design and optimization of universal light-emitting material candidates in optoelectronic devices.

Introduction

Colour temperature (CT) is a characteristic of visible light that has important applications in lighting, photography, manufacturing and other fields.[1] Interestingly, higher colour temperatures (CTs) exhibit cooler colours, while lower CTs exhibit warmer colours. Therefore, different CTs produce different effects on human physiology and psychology, which may be harmful or beneficial.[2,3] Among many types of light sources, light emitting diodes (LEDs) are attracting considerable attention because their luminescence is similar to natural light sources. LEDs with low CTs are proven to be helpful in protecting the ocular surface, ameliorating insomnia, promoting the secretion of melatonin and glutamate, accelerating wound healing and hair regeneration, and are very suitable as healthy indoor light sources.[4,5]

With the continuous improvement of people's requirements for life quality, creating human-friendly LEDs with low CTs like sunset or candlelight is highly desirable. In recent years, Jou *et al.*,[6] Gong *et al.*[7] and Korshunov *et al.*[8] reported candle light-style organic LEDs with CTs as low as 1900 K, 1843 K and 1722 K, respectively. However, there are few reports on the photophysical properties of luminescent materials with CTs lower than candlelight, so it is necessary to further strengthen the basic research on the preparation strategies and photophysical mechanisms of such materials. More noteworthy, if such materials also have good two-photon absorption (TPA) characteristics, they will have wider potentials in the fields of two-photon fluorescence microscopy, optical data storage and thermodynamic therapy.

Herein, we compare the photophysical properties of four fluorenone-based conjugated oligomers: 2,7-di(4-(diphenylamino)styryl)-9-fluorenone (#1), 2,7-di((*E*)-2-(10-octyl-10*H*-phenothiazin-3-yl)vinyl)-9-fluorenone (#2), 2,7-di((*E*)-2-(7-(4-(diphenylamino)styryl)-9,9-dioctyl-9*H*-fluoren-2-yl)vinyl)-9-fluorenone (#3) and 2,7-di((*E*)-2-(9,9-dioctyl-7-((*E*)-2-(10-octyl-10*H*-phenothiazin-3-yl)vinyl)-9*H*-fluoren-2-yl)vinyl)-9-fluorenone (#4). The structure–property relationships are analyzed by performing a variety of steady-state and transient spectral measurements. Meanwhile, the transition dipole moments and TPA cross sections are simulated by using sum-over-essential states (SOS) approach. We observe that the electron-donating and withdrawing groups directly linked oligomers present CTs lower than 1700 K, while the incorporation of spacer units could weaken the role of electron-donating groups and effectively enhance the TPA performance of oligomers. It is hoped that our research will provide suitable candidates for the design and fabrication of light-emitting materials in photoelectric devices with low CTs and good two-photon performance.

[a]*Department of Science, Zhijiang College of Zhejiang University of Technology, Shaoxing 312030, China. E-mail: hth@zzjc.edu.cn; xutianning@zjut.edu.cn*

[b]*Griffith Business School, Griffith University, Parklands Dr, Southport, QLD 4215, Australia*

[c]*College of Chemistry, Jilin University, Changchun 130012, China*

[d]*Jiangsu Sino-tech Polym. New Materials Industry Technology Research Institute Co., Ltd., Changzhou 213000, China. E-mail: zhouhuipeng0318@163.com*

† Electronic supplementary information (ESI) available. See DOI: https://doi.org/10.1039/d3ra00083d

Experimental

Materials

The conjugated oligomers #1, #2, #3 and #4 were synthesized following Heck reaction,[9] and the synthetic procedures have been described in detail previously.[10–12] As seen in Fig. 1, for #1 and #2, triphenylamine and phenothiazine serve as the electron-donating groups, are linked to fluorenone directly. While for #3 and #4, fluorene–ethylene units are inserted between electron-donating and withdrawing groups. Toluene solutions with concentrations at 5×10^{-5} and 5×10^{-4} M were prepared for one- and two-photon measurements, respectively. All the measurements were carried out at room temperature, with the samples placed in 3 mm path length quartz cells.

Measurements

Mass spectra were performed on Agilent 1100 MS series and AXIMA CFR matrix assisted laser desorption ionization/time of flight (MALDI/TOF) mass spectrometer. The ^{1}H-NMR spectra were recorded in $CDCl_3$ on a 500 MHz NMR spectrometer (JEOL, JNM-500EX). C, H and N elemental analyses were taken on a elemental analyzer (PerkinElmer, 240C). The infrared (IR) spectra were measured using a FT-IR spectrometer (Bruker, VERTEX 80v) by incorporating samples in KBr disks. The steady-state absorption spectra were measured by a bi-pass fiber spectrometer (Avantes, AvaSpec-2048). One-photon fluorescence (OPF) measurements were carried out by use of a fiber optic spectrometer (Ocean Optics 4000). Two-photon fluorescence (TPF) and two-colour pump–probe experiments were carried out with Ti:sapphire mode-lock femtosecond laser system (Coherent), which consists of pumping source (Verdi-V5), oscillator stage (Mira 900), amplifier stage (Legend Elite) and optical parametric amplifier (Topas). The centered wavelength of the pulses from the oscillator stage is 800 nm, with average power of 600 mW, repetition rate of 76 MHz, and pulse width of 110 fs. When the pulses passed through the amplifier stage, the repetition rate becomes 1 kHz, and the single pulse energy becomes 3.5 mJ.

Results and discussion

The structures of the conjugated oligomers were characterized by MALDI/TOF mass spectroscopy, ^{1}H-NMR, elemental analysis and IR spectra. By utilizing 1,8,9-trihydroxyanthracene as a matrix, molecular ion peaks of target molecules could be clearly observed, as shown in Fig. 1. However, due to the existence of oxygen free radicals in the environment, which are easy to bind with lone-pair electrons on phenothiazine units, regular oxygen-rich molecular ion peaks could be observed in #2 and #4. The data of ^{1}H-NMR and elemental analysis are available in the ESI (S1†). The 500 MHz ^{1}H-NMR spectra exhibit that no signal corresponding to the protons in *cis*-double bonds at 6.5 ppm appeared in all the target compounds (Fig. S1, ESI†).

Fig. 2 shows the IR spectra of compound #1–#4. The frequencies and assignments of characteristic vibrational peaks are listed in Table 1. The oligomers exhibit obvious CH_2 asymmetrical stretching (υ_{as} CH_2) and symmetrical stretching (υ_s CH_2) vibration intensity due to their massive methylene groups. When fluorene–ethylene units are introduced into #1 and #2, the characteristic peaks of keto-carbonyl (υ C=O)[13] are weakened obviously, implying that spacer groups inhibited the

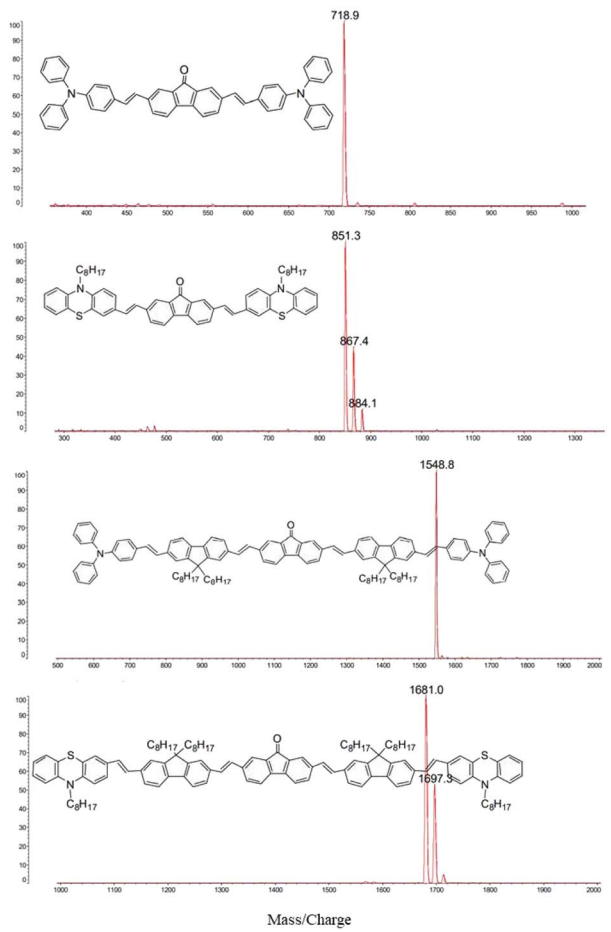

Fig. 1 The MALDI/TOF MS spectra of compound #1–#4 with 1,8,9-trihydroxyanthracene as a matrix.

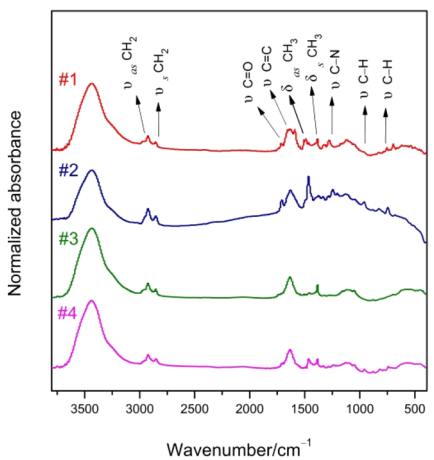

Fig. 2 IR spectra of compound #1–#4.

Table 1 Characteristic vibrational frequencies and their assignment of oligomers

	Vibrational frequencies/cm^{-1} (relative strength/%)			
Assignment	#1	#2	#3	#4
υ_{as} CH_2	2923 (9.9)	2925 (20.6)	2925 (13.6)	2924 (12.5)
υ_{s} CH_2	2855 (7.4)	2851 (11.0)	2854 (8.5)	2851 (8.2)
υ C=O	1715 (10.1)	1707 (15.8)	1719 (6.1)	1703 (6.1)
υ C=C	1635 (27.4)	1630 (24.2)	1635 (29.4)	1634 (27.9)
δ_{as} CH_3	1463 (8.3)	1467 (43.4)	1457 (3.3)	1461 (11.9)
δ_{s} CH_3	1385 (14.3)	1385 (6.4)	1385 (14.3)	1382 (11.1)
δ =C–H	964 (5.5)	958 (8.4)	960 (2.5)	960 (5.1)
δ =C–H	754 (5.9)	739 (8.6)	753 (1.9)	741 (5.4)
υ C–N	1281 (9.5)	1247 (10.3)	1270 (1.3)	1246 (2.6)

vibration ability of the electron-withdrawing groups. Besides, the stretching vibration peaks of C=C (υ C=C) are enhanced with C=C prolonging. The characteristic C–N stretching (υ C–N) frequencies show a red-shift with the electron-donating groups change from triphenylamine to phenothiazine, and the peak intensities are strongly weakened by the introduction of spacer groups. The characteristic band of thiophene is located around 600–800 cm^{-1}. It is noteworthy that the oligomers exhibit IR absorption bands near 960 cm^{-1} arising from the wagging vibration of the *trans*-double bond (CH=CH),[14] but no characteristic absorption was observed at the vibration position of the *cis*-double bond at 830 cm^{-1}. Therefore, we confirm that all the double bonds in the synthesized oligomers are *trans* configurations. The *trans*-form compounds have good planarity, which is beneficial to the improvement of the fluorescence property.

The steady-state absorption spectra of oligomers dissolved in toluene (5×10^{-5} M) are shown in Fig. 3. Absorption bands in the ultraviolet region around 320 nm should be ascribed to the n–π* transitions of heteroatoms in triphenylamine and phenothiazine moieties, the high intensity peaks near 420 nm can be assigned to π–π* electronic transitions of the conjugated molecules,[15] and the 480–500 nm shoulder bands could be attributed to intramolecular charge transfer (ICT) from electron-donating to withdrawing groups.[16,17] Spectral parameters obtained by employing multi-peaks Gaussian fit are summarized in Table S1 (ESI†). The n–π* band of #2 possesses larger percentage owing to the electron-rich nitrogen and sulfur heteroatoms which favor n–π* transition. It is worth noting that #2 also exhibits larger area percentage of ICT, as compared with #1, indicating the electron-donating ability of phenothiazine is stronger than that of triphenylamine, due to its electron-rich tricyclic heteroarene with nonplanar butterfly structure.[18] However, the insertion of fluorene–ethylene units resulted in a much smaller ICT area percentage for #3 and #4, because of the spacer groups effectively increase the conjugated length of the molecule, making the distance between the electron-donating and withdrawing groups obviously larger. The similar spectral parameters between #3 and #4 also indicate that the fluorene–ethylene spacer groups can eliminate the difference between the spectral behaviors of oligomers with different electron-donating groups. The normalized steady-state absorption and OPF spectra are together shown in Fig. S2 (ESI†) for comparison, with the corresponding linear optical parameters summarized in Table S2 (ESI†). Compared to #1 and #2, the absorption maximum of #3 and #4 shows a red-shift of ~15 nm, indicating a more conjugated feature. The OPF spectra of #1 and #2 exhibit structureless band, and there is a 10 nm bathochromic shift with the electron-donating groups change from triphenylamine to phenothiazine, which could be attributed to the enhancement of the ICT. When it comes to #3 and #4, introducing of spacer groups resulted in blue-shift of the emission peak, in accompany with a new emerging shoulder band at ~610 nm, which may originate from the fluorene-based characteristic emission. The Stokes shift presents a trend of #2 > #1 > #3 ≈ #4, indicating an enhanced ICT character[19] occurs in phenothiazine end-capped oligomer #2, and the ICT between electron-donating and withdrawing groups could be inhibited by the inserted π-spacer groups. The optical bandgap E_g^{opt} shows opposite trend of #2 < #1 < #3 = #4, which further validates the above inference.

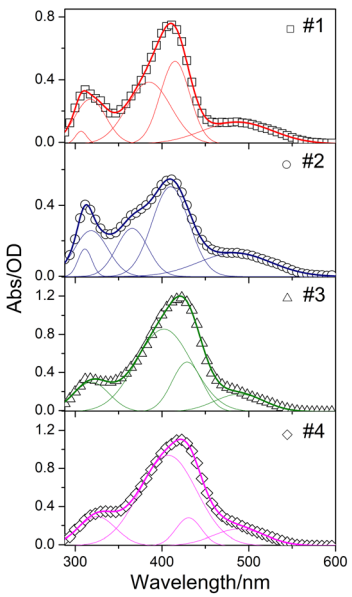

Fig. 3 Steady-state absorption spectra of compound #1–#4. The solid lines represent the fitted Gaussian line-shape.

#1 and #2 exhibited reddish orange luminescence with spectral maxima at 597 and 607 nm, respectively. With the incorporation of fluorene–ethylene spacers, the emission maxima of #3 and #4 were hypsochromic shifted by 24 and 36 nm respectively relative to #1 and #2, and the luminescence colour became yellowish orange. The colour coordinates of oligomers in International Commission on Illumination (CIE) are presented in Fig. 4. The colour coordinates are located near the border of CIE, which is indicative of high colour saturation. Through the coordinates, correlated CTs of #1–#4 are calculated to be 1686, 1699, 2350 and 2331 K. #1 and #2 present extremely low CTs, which are even lower than those of matchstick flame, candlelight and sunset/sunrise (1700–1800 K). Although the CTs of #3 and #4 are higher as compared with #1 and #2, they are still lower than those of incandescent light bulb, studio lamps and photofloods (2700–3300 K). Meanwhile, #3 and #4 exhibit

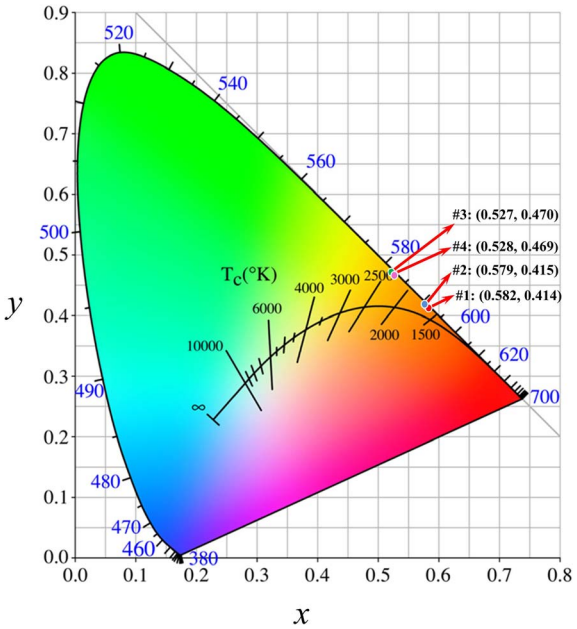

Fig. 4 CIE coordinates and CTs of #1–#4.

about 2.5–2.6 times enhancement in the whole emission intensity owing to the incorporation of π-spacer units.

We have demonstrated that these oligomers are suitable candidates for low CT optoelectronic devices. Furthermore, if these materials also have excellent TPA properties, they will have wider applications in many fields. To investigate the nonlinear optical properties, we measure the TPF spectra at different laser intensities from 35 to 80 μJ under the femtosecond laser pulses of 800 nm. Fig. 5(a) shows the normalized TPF spectra of oligomers in toluene (5×10^{-4} M). The TPF

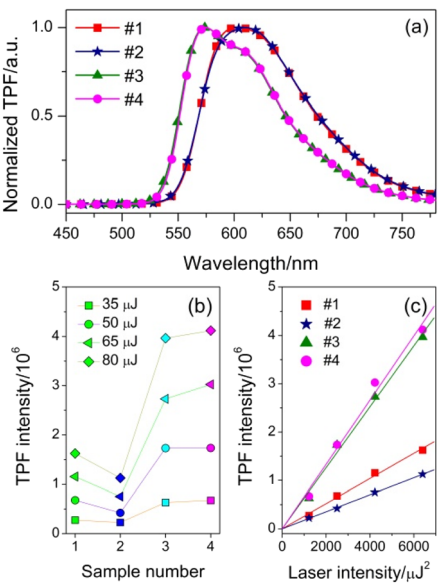

Fig. 5 (a) Normalized TPF spectra of #1–#4 (5×10^{-4} M); (b) TPF intensity of #1–#4 at different laser intensities over a range of 35–80 μJ; (c) TPF intensity as a function of the square of laser intensity.

maxima are located at 605, 610, 574 and 574 nm for #1, #2, #3 and #4 respectively, which are slightly red-shifted relative to those of OPF, because of the reabsorption effect.[20] The spectral line shapes of TPF are the same as those of the OPF, suggesting that the emission state does not change and that we can simulate the nonlinear optical parameters by linear optical spectra. The plots of integrated TPF intensity *versus* sample number are depicted in Fig. 5(b). For all the oligomers, the TPF intensities are gradually increased with increasing laser intensity. At the same laser intensity, the stronger ICT character of #2 leads to fluorescence quenching compared to #1, due to the stronger electron-donating capacity of phenothiazine units. However, the difference between the TPF intensity of #3 and #4 is much smaller than that between #1 and #2 when the fluorene–ethylene spacers were introduced. More importantly, the TPF intensity could be significantly enhanced with the increase of conjugated length. The laser intensity-dependent integrated TPF intensity of oligomers is shown in Fig. 5(c). A clear linear dependence of the TPF intensity on the square of laser intensity is strong indication that the 800 nm excited fluorescence could be assigned to TPA process. According to the slopes of linear fitted lines, the TPF efficiency of #3 and #4 increases about 2.4- and 3.8-fold compared to their counterparts without fluorene–ethylene spacers. Meanwhile, the difference of TPF efficiency between triphenylamine and phenothiazine end-capped oligomers is significantly reduced, and the ratios before and after the introduction of π-spacers are 3 : 2 (#1 : #2) and 10 : 11 (#3 : #4), respectively.

TPA cross section is an important parameter in quantifying the TPA abilities of compounds.[21,22] Since TPF and OPF come from the same emission state as mentioned above, linear absorption spectra can be used to simulate the TPA cross section and other corresponding parameters of oligomers by exploiting SOS approach derived from semi-classical time-dependent perturbation theory.[23] All calculations are performed in centimeter-gram-second system of electromagnetic units. Assuming that the absorption spectra exhibit Gaussian line-shape[24,25]

$$g_{0m}(\nu) = \sqrt{\frac{4\ln 2}{\pi}}\,\frac{A_{0m}}{\Gamma_{0m}}\exp\left[-4\ln 2\left(\frac{\nu_{0m}-\nu}{\Gamma_{0m}}\right)^2\right] \quad (1)$$

where A_{0m}, Γ_{0m} and υ_{0m} are the peak height, full width at half-maximum and peak frequency in the fitted Gaussian line-shape. Moreover, Γ_{0m} corresponds to the damping constant of the m state, υ_{0m} corresponds to the transition frequency between the m and the ground state.

Assuming the excitation light is linearly polarized and therefore the dipole moments are parallel, the transition dipole moment of transition from the ground to m state can be calculated using:[26]

$$\mu_{0m} = \sqrt{\frac{3}{4\pi}\,\frac{c}{\pi^{1/2}\sigma_{0m}^{max}}\,\frac{\Gamma_{0m}}{2(\ln 2)^{1/2}}\,\frac{h}{\nu_{0m}}} \quad (2)$$

where σ_{m0}^{max} is the maximum one-photon absorption cross section that can be calculated by $\sigma_{m0}^{max} = \varepsilon \ln 10/N_A$, where ε is the molar absorption coefficient, N_A is the Avogadro's constant.

The absorption spectra are well fitted with sum of multi-Gaussian, as shown by the solid lines in Fig. 3. According to the results of Gaussian fitting, we assume that the oligomers whose electron-donating and withdrawing moiety connected directly have one initial state ($|S_0\rangle$), one intermediate state ($|S_1\rangle$) and four final states ($|S_2\rangle$–$|S_5\rangle$), while the spacer introduced counterparts have one initial state ($|S_0\rangle$), one intermediate state ($|S_1\rangle$) and three final states ($|S_2\rangle$–$|S_4\rangle$). Then the TPA cross section can be expressed as:[27]

$$\sigma^{(2)} = \frac{4}{5\pi}\frac{(2\pi)^4}{(ch)^2}\frac{{\nu_p}^2}{\left(\nu_{01}-\nu_p\right)^2+{\Gamma_{01}}^2}\sum_{m=2}^{n}\left[\frac{|\mu_{1m}|^2|\mu_{01}|^2\Gamma_{0m}}{\left(\nu_{0m}-2\nu_p\right)^2+{\Gamma_{0m}}^2}\right] \quad (3)$$

where υ_p is the frequency of laser, $|\mu_{1m}| = |\mu_{0m} - \mu_{01}|$. The obtained spectroscopic parameters are summarized in Table 2.

The multi-energy-level diagrams for compound #1–#4 under the SOS approach are depicted in Fig. 6. Consistent with the absorption spectra, the $|S_1\rangle$ state represents the ICT state, while the higher states represent the localized-excited states. The transition dipole moments between the $|S_0\rangle$ and $|S_1\rangle$ (μ_{01}) are lower for #3 and #4, probably due to the introduction of fluorene–ethylene spacer, whose electron-donating ability is weaker than that of triphenylamine and phenothiazine, thus inhibiting the interaction between electron-donating and withdrawing groups. However, the μ_{13} and μ_{14} are higher for #3 and #4, because of their larger conjugated length.[23] The values of theoretical TPA cross section ($\sigma_T^{(2)}$) obtained using eqn (3) are 986, 754, 1658, 1766 GM, the experimental TPA cross section ($\sigma_E^{(2)}$) values achieved by z-scan technique in previous studies[11,12] are also listed in Table 2 for comparison. It is obvious that the incorporating of fluorene–ethylene units could lead to 170–230% enhancement of TPA cross section.

After a molecule is in thermodynamic equilibrium with the solvent, it will relax to an ICT state. The relaxation process of ICT state is accompanied by fluorescence emission and usually completed in hundreds of picoseconds. To better understand

Table 2 Spectroscopic parameters obtained by the SOS approach, employing the multi-energy-level diagram

TPA parameters	#1	#2	#3	#4
υ_{01}/cm^{-1}	20 553	20 684	20 462	20 467
υ_{02}/cm^{-1}	24 113	24 416	23 330	23 236
υ_{03}/cm^{-1}	25 990	27 368	24 885	24 577
υ_{04}/cm^{-1}	31 526	31 437	31 399	30 778
υ_{05}/cm^{-1}	32 625	32 162		
Γ_{01}/cm^{-1}	3437	3594	2404	2534
Γ_{02}/cm^{-1}	1987	2554	1905	1577
Γ_{03}/cm^{-1}	3414	2707	3979	3998
Γ_{04}/cm^{-1}	3589	3817	4083	4095
Γ_{05}/cm^{-1}	1390	1635		
μ_{01}/debye	9.8	9.8	7.4	7.3
μ_{12}/debye	3.6	5.0	2.9	0.3
μ_{13}/debye	4.8	0.8	11.1	12.2
μ_{14}/debye	1.8	1.6	2.6	2.7
μ_{15}/debye	6.0	4.1		
$\sigma_T^{(2)}$/GM	986	754	1658	1766
$\sigma_E^{(2)}$/GM	884	781	1759	1743

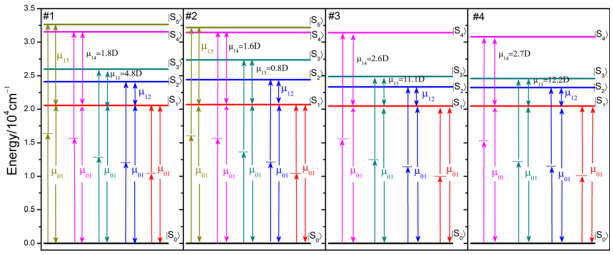

Fig. 6 Multi-energy-level diagrams for compound #1–#4 used to describe the TPA process under the SOS approach.

the ICT dynamics influenced by the electron-donating capacity and π-spacer units, two-color pump–probe experiment has been performed. Schematic illustration of the two-color pump–probe system is shown in Fig. 7(a). The amplified 800 nm laser beam is separated into two beams. The stronger one pumps the Topas which serves as a tunable source, and the other one is used as the probe beam. The pump beam is chopped with a chopper at a rate of 410 Hz and focused onto the sample cuvette after

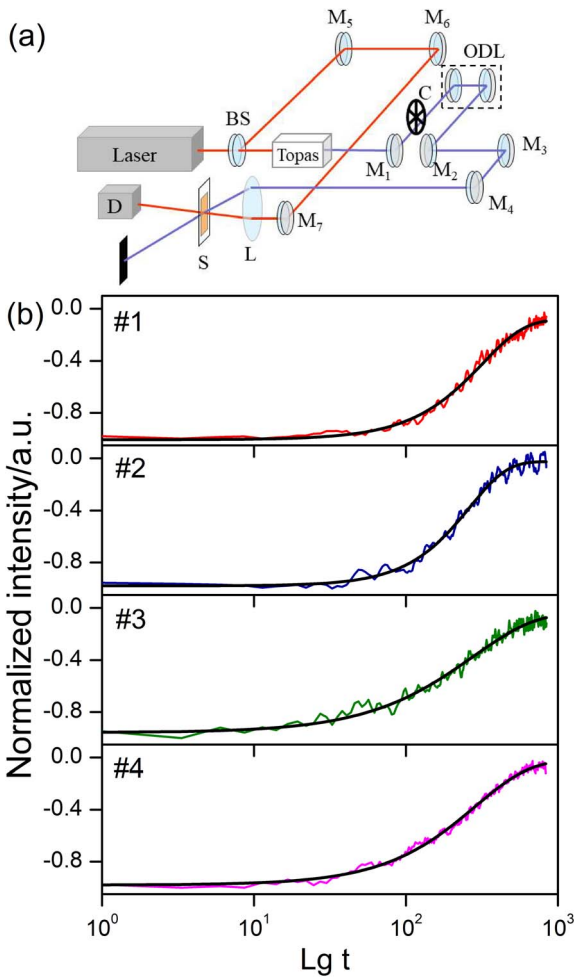

Fig. 7 (a) Schematic of the two-colour pump–probe system. BS is beam splitter; M_1–M_7 are mirrors; C is chopper; L is convex len; S is sample; and D is photodiode detector; (b) two-color pump–probe dynamics for sample solutions at excitation of 410 nm.

passing through an optical delay line (ODL), the probe beam is also focused and overlapped with the pump beam. The signal of transmittance change is collected by a photodiode connected with a lock-in amplifier (SR830 DSP) and finally recorded on a computer. Photoexcitation is carried out at 410 nm, corresponding the lowest energy π–π* transition.[28] The absorption decay traces were measured with a probe wavelength at 800 nm. The results of two-color pump–probe dynamics together with fitting curves are shown in Fig. 7(b). Logarithm of the decay time is taken as the abscissa. Considering the multiformity of transient decay processes, we exploit the stretched exponential,[29] which can be expressed as:

$$\Delta \mathrm{OD} \propto \exp\left[-\left(\frac{t}{\tau}\right)^{\alpha}\right] \quad (4)$$

where t is the time, τ is the lifetime of the transients, and α is the stretching exponent. So the mean lifetime ($\langle\tau\rangle$) can be calculated by using function of $\langle\tau\rangle = (\tau/\alpha)\Gamma(1/\alpha)$, $\Gamma(1/\alpha)$ can be derived from gamma function.[30] The fitted lifetime results attributed to ICT are as follows: 287 ps (#1), 234 ps (#2), 267 ps (#3) and 268 ps (#4). The phenothiazine end-capped oligomer #2 shows shorter decay time than its triphenylamine end-capped counterpart #1, it is evident that the ICT is enhanced and accelerated due to the increase of electron-donating ability. However, #3 and #4 show an interesting result that their mean lifetimes are extremely similar. The reason for this phenomenon is that the inserted fluorene–ethylene moieties weaken the role of electron-donating groups and inhibited the ICT behavior to some extent.

Conclusions

In summary, one- and two-photon optical properties of four fluorenone-based conjugated oligomers have been experimentally and theoretically analysed in detail. The emission of triphenylamine and phenothiazine end-capped oligomers could present extremely low CTs, which are even lower than 1700 K. The spectral line-shape, peak position, TPF efficiency and ICT lifetime are all modulated by electron-donating capacity and introduction of π-spacer units. The TPA cross section and other corresponding parameters of oligomers have been calculated exploiting SOS approach. The results suggest that phenothiazine groups with stronger electron-donating ability could increase the ICT behavior of oligomers in which the electron-donating and withdrawing groups are directly linked. However, the introduction of fluorene–ethylene spacers could inhibit the interaction between electron-donating and withdrawing groups. Because of the larger conjugated length, fluorene–ethylene spacers could also effectively enhance the TPA performance of oligomers. This study would be helpful for the design and optimization of photoelectric materials with both low colour temperature and excellent two-photon optical properties.

Conflicts of interest

There are no conflicts to declare.

Acknowledgements

This work was supported by Zhejiang Provincial Natural Science Foundation of China (LQ19F050004).

Notes and references

1 A. K. R. Choudhury, *Principles of Colour and Appearance Measurement*, Woodhead Publishing Limited, Cambridge, 2014.
2 K. Choi, C. Shin, T. Kim, H. J. Chung and H.-J. Suk, *Sci. Rep.*, 2019, **9**, 345.
3 P. R. Mills, S. C. Tomkins and L. J. M. Schlangen, *J. Circadian Rhythms*, 2007, **5**, 2.
4 M. Jin, X. F. Li, F. Yan, W. X. Chen, L. Jiang and X. Zhang, *J. Photochem. Photobiol., B*, 2021, **214**, 112099.
5 J. Q. Lin, X. W. Ding, C. Hong, Y. L. Pang, L. M. Chen, Q. W. Liu, X. Zhang, H. B. Xin and X. L. Wang, *Sci. Rep.*, 2019, **9**, 7560.
6 J.-H. Jou, C.-Y. Hsieh, J.-R. Tseng, S.-H. Peng, Y.-C. Jou, J. H. Hong, S.-M. Shen, M.-C. Tang, P.-C. Chen and C.-H. Lin, *Adv. Funct. Mater.*, 2013, **23**, 2750–2757.
7 Y. Y. Gong, J. Liu, Y. R. Zhang, G. F. He, Y. Lu, W. B. Fan, W. Z. Yuan, J. Z. Sun and Y. M. Zhang, *J. Mater. Chem. C*, 2014, **2**, 7552–7560.
8 V. M. Korshunov, T. N. Chmovzh, E. A. Knyazeva, I. V. Taydakov, L. V. Mikhalchenko, E. A. Varaksina, R. S. Saifutyarov, I. C. Avetissov and O. A. Rakitin, *Chem. Commun.*, 2019, **55**, 13354–13357.
9 R. F. Heck and J. P. Nolley, *J. Org. Chem.*, 1972, **37**, 2320.
10 T.-H. Huang, D. Yang, Z.-H. Kang, E.-L. Miao, R. Lu, H.-P. Zhou, F. Wang, G.-W. Wang, P.-F. Cheng, Y.-H. Wang and H.-Z. Zhang, *Opt. Mater.*, 2013, **35**, 467–471.
11 T.-H. Huang, X.-C. Li, Y.-H. Wang, Z.-H. Kang, R. Lu, E.-L. Miao, F. Wang, G.-W. Wang and H.-Z. Zhang, *Opt. Mater.*, 2013, **35**, 1373–1377.
12 T.-H. Huang, J.-Q. Hou, Z.-H. Kang, Y.-H. Wang, R. Lu, H.-P. Zhou, X. Zhao, Y.-G. Ma and H.-Z. Zhang, *J. Photochem. Photobiol., A*, 2013, **261**, 41–45.
13 W.-Y. Wong, G.-L. Lu, K.-H. Choi and Z. Y. Lin, *Eur. J. Org. Chem.*, 2003, **2003**, 356–373.
14 X. P. Qiu, R. Lu, H. P. Zhou, X. F. Zhang, T. H. Xu, X. L. Liu and Y. Y. Zhao, *Tetrahedron Lett.*, 2007, **48**, 7582–7585.
15 H. Hoppe and N. S. Sariciftci, *J. Mater. Res.*, 2004, **19**, 1924–1945.
16 J. L. Segura, N. Martín and D. M. Guldi, *Chem. Soc. Rev.*, 2005, **34**, 31–37.
17 F. Garnier, *Acc. Chem. Res.*, 1999, **32**, 209–215.
18 Y. Rout, C. Montanari, E. Pasciucco, R. Misra and B. Carlotti, *J. Am. Chem. Soc.*, 2021, **143**, 9933–9943.
19 A. Bhaskar, G. Ramakrishna, Z. K. Lu, R. Twieg, J. M. Hales, D. J. Hagan, E. Van Stryland and T. Goodson, *J. Am. Chem. Soc.*, 2006, **128**, 11840–11849.
20 L. Z. Wu, X. J. Tang, M. H. Jiang and C. H. Tung, *Chem. Phys. Lett.*, 1999, **315**, 379–382.
21 Y. C. Wang, Y. Z. Wang, G. Q. Wang and D. J. Liu, *Optik*, 2018, **172**, 186–190.

22 M. Sheik-Bahae, A. A. Said, T.-H. Wei, D. J. Hagan and E. W. Van Stryland, *IEEE J. Quantum Electron.*, 1990, **26**, 760–769.
23 M. G. Vivas, S. L. Nogueira, H. Santos Silva, N. M. Barbosa Neto, A. Marletta, F. Serein-Spirau, S. Lois, T. Jarrosson, L. De Boni, R. A. Silva and C. R. Mendonca, *J. Phys. Chem. B*, 2011, **115**, 12687–12693.
24 L.-J. Gong, Y.-H. Wang, Z.-H. Kang, T.-H. Huang, R. Lu and H.-Z. Zhang, *Chin. J. Chem. Phys.*, 2012, **25**, 643–648.
25 T.-H. Huang, Y.-H. Wang, T.-N. Xu, F.-Y. Yu, H.-Z. Zhang and Y.-R. Wang, *Chin. J. Chem. Phys.*, 2015, **28**, 557–562.
26 P. N. Day, K. A. Nguyen and R. Pachter, *J. Phys. Chem. B*, 2005, **109**, 1803–1814.
27 K. Kamada, K. Ohta, Y. Iwase and K. Kondo, *Chem. Phys. Lett.*, 2003, **372**, 386–393.
28 R. Siebert, D. Akimov, M. Schmitt, A. Winter, U. S. Schubert, B. Dietzek and J. Popp, *ChemPhysChem*, 2009, **10**, 910–919.
29 D. C. Elton, Stretched Exponential Relaxation, *arXiv*, 2018, preprint, arXiv:1808.00881, DOI: **10.13140/RG.2.1.5109.5287**.
30 W. Freeden and M. Gutting, *Special Functions of Mathematical (Geo-)Physics*, Springer, Basel, 2013.